

We are IntechOpen, the world's leading publisher of Open Access books Built by scientists, for scientists

6,900

Open access books available

186,000

International authors and editors

200M

Downloads

Our authors are among the

154

Countries delivered to

TOP 1%

most cited scientists

12.2%

Contributors from top 500 universities



WEB OF SCIENCE™

Selection of our books indexed in the Book Citation Index
in Web of Science™ Core Collection (BKCI)

Interested in publishing with us?
Contact book.department@intechopen.com

Numbers displayed above are based on latest data collected.
For more information visit www.intechopen.com



Viscoelasticity of a Supramolecular Polymer Network and its Relevance for Enhanced Oil Recovery

Laura Romero-Zerón and Saran Banthong

Additional information is available at the end of the chapter

<http://dx.doi.org/10.5772/intechopen.77277>

Abstract

Supramolecular polymer networks are built up by combining multiple noncovalent interactions among macromolecules, resulting in the formation of materials with versatile functionality. This chapter describes an exploratory research focused on the formulation of a supramolecular polymer network based on reversible interactions among the main- and side chains of a mixture of xanthan gum, partly hydrolyzed polyacrylamide (HPAM), and a hydrophobically modified polyacrylamide (HMPAM) in brine solutions relevant for applications in enhanced oil recovery (EOR). The formation and characterization of the supramolecular network system was carried out through oscillatory rheology.

Keywords: supramolecular polymers, self-assembling, self-association, polymer flooding, heavy oil recovery, salt tolerance, mechanical stability, thermal stability

1. Introduction

Self-organization of molecular structures refers to the spontaneous assembly of individual building blocks into ordered and thermodynamically stable nanostructures by noncovalent interactions, resulting in the formation of dynamic and responsive materials. The noncovalent (reversible) interactions include electrostatic attractions, metal/ligand complexes, π/π -stacking, ionic interactions, hydrogen bonding, or hydrophobic effects without the application of external energy. Therefore, self-assembly is a low-cost and high-yield process [1–6] that can be activated by external stimuli, which involves changes in temperature, pH, ionic strength, radiation, the addition of other molecules, or their combination [2, 7–9].

Supramolecular polymer networks can be formed by polymer blends (PBs) in which the reversible and highly directional noncovalent interactions are randomly distributed across the polymer chains [6]. The resulting supramolecular structure displays polymeric properties in dilute and concentrated solutions that follow well-established theories of polymer physics [9]. These networks exhibit enhanced material properties compared to the individual polymers [1], and the reversibility of noncovalent interactions provides self-healing properties to these materials [6, 10].

This study focuses on the formulation and characterization of a supramolecular polymer network based on reversible interactions among the main- and side chains of a mixture of xanthan gum, HPAM, and HMPAM or associating polymer (AP) in brine. Xanthan gum and HPAM are the most commonly used polymers in the field for enhanced oil recovery (EOR) [11]. **Figure 1** displays the chemical structures of these polymers.

Xanthan gum is a high-molecular weight ($\approx 2\text{--}3 \times 10^6$ g/mol) anionic polysaccharide derived from the fermentation of the bacterium *Xanthomonas campestris*. Its chemical structure contains a cellulose backbone consisting of five monosaccharides to form a pentasaccharide repeating unit. The cellulosic backbone is substituted at C-3 on alternate β -1,4-D-glucopyranosyl residues with charged trisaccharide side chains of β -D-rhamnopyranosyl β -1,4-D-glucuronopyranosyl, and α -1,2-D-mannopyranosyl. The two charged functional groups, COO^- , are found in the α -Manp and β -GlcAp residues (**Figure 1(a)**) [8, 11–25].

Xanthan gum is a stereoregular polymer and displays order–disorder transition in solution that depends on polymer concentration, ionic strength, and temperature [11–14, 17, 19, 24, 26]. A high polymer concentration and an increased ionic strength support ordered structures, while elevated temperatures favor disorder structures [11]; therefore, xanthan gum is a thermally responsive biopolymer [27]. At low temperatures, the native state of xanthan gum shows an ordered and rigid conformation as a single helical or a double-strand helix stabilized by inter- and intramolecular hydrogen bonds. The ordered conformation of the xanthan molecule is semi-flexible with a hydrodynamic length ranging from 600 to 2000 nm and a hydrodynamic diameter of 2 nm [20]. At elevated temperatures ($\geq 60^\circ\text{C}$) [12, 16, 24] and low ionic strength, the native state, which displays an order state, transitions to a more flexible disordered-denatured state [13]. Optical rotation measurements have demonstrated that xanthan gum dissolved in distilled water at 25°C displayed the nonordered conformation [24]. However, a decrease in temperature ($<40^\circ\text{C}$) [16, 24, 28] and the simultaneous increase in the ionic strength cause

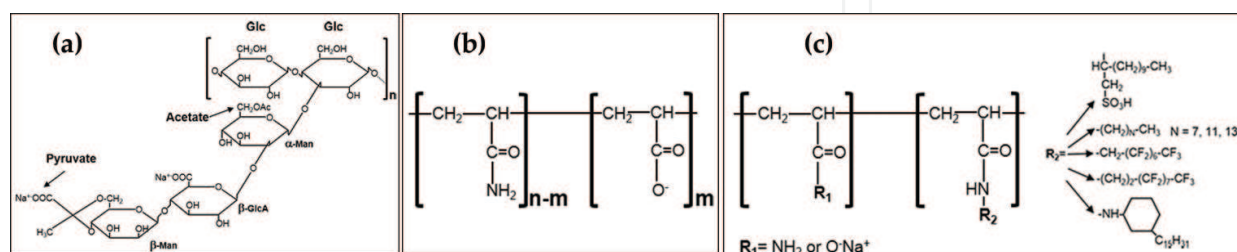


Figure 1. Generic chemical structures of (a) xanthan gum, (b) HPAM, and (c) associating polymers (**Figure 1(a)** was adapted from reference [12] and **Figure 1(b)** and **(c)** were adapted from reference [13]).

conformation reversal to a reordered-renatured state [11–19, 21–23, 27, 29, 30]. In saline solutions, monovalent or divalent cations (e.g., Na^+ and Ca^{2+}) condense on the ionized carboxyl moieties on the xanthan trisaccharide side chains, reducing repulsive forces between polymer chains. The side chains collapse down to the backbone causing conformation transition to a rigid rod-like shape of reduced hydrodynamic size stabilized by hydrogen bonding [23]. This conformation increases the intra- and intermolecular attraction and the xanthan chains tend to adopt a more rigid ordered conformation [13, 14]. The stability of xanthan gum is attributed to its ordered conformation which is stabilized by salts. Thus, the optimum functionality of xanthan gum requires the addition of salt [17].

Xanthan gum is prone to self-association at low concentrations and has been used as a building block to generate self-assembled structures [24, 25]. The onset of macromolecular self-organization has been reported at concentrations ≥ 0.1 wt% [8]. Parallel packing or side-by-side associations stabilized by hydrogen bonds facilitate the formation of three-dimensional networks [8, 19, 26]. Previous research has also demonstrated the self-organization of xanthan gum through polyelectrolyte complexation with other polysaccharides, such as chitosan-xanthan, β -lactoglobulin-xanthan, α -galactosidase-modified guar gum-xanthan, and sodium caseinate-xanthan, among many others [8, 26, 31]. Another example of self-aggregation through hydrophobic interactions is the intermolecular binding of xanthan gum-carob gum. These self-organizations take place in both the ordered and disordered conformations of the xanthan macromolecule depending on the ionic strength [8, 20, 32, 33].

Advantages of xanthan gum include non-toxicity, high water solubility, salinity tolerance, stability over a broad range of pH values, thermal stability against hydrolysis provided by its ordered conformation, high shear stability, high viscosities but a significant shear-thinning behavior on shearing at a low concentration, slight variations in viscosity with changes in temperature, availability, the ease of processing, and low manufacturing costs [11, 17, 18, 22, 26, 34, 35]. The main downside of xanthan gum is high sensitivity to microbial attack. Salt-tolerant aerobic and anaerobic microorganisms can degrade the xanthan gum chains leading to loss in solution viscosity. In practical applications, biocides are added to the xanthan gum solution to suppress the growth of degrading microorganisms [11, 17, 36].

Partially hydrolyzed polyacrylamides, HPAMs (**Figure 1(b)**), with degree of hydrolysis ranging from 25 to 35%, are the most used polymers for enhanced oil recovery (EOR) [35, 37]. HPAM is highly sensitive to mono- and divalent cation environments because of the shielding effect of the negative charges on the polymer backbone. Thus, the static repulsion between the HPAM lateral groups fades and the polymer structure collapses, which drastically reduces the viscosity of the polymer solution [35]. Divalent cations (e.g., Ca^{2+}) can also induce the self-aggregation of HPAM through polyion-cation complexation and depending on the concentration of Ca^{2+} inter- and intrachain complexation takes place [36]. The molecular conformation and viscosity of HPAM solutions are also affected by the degree of hydrolysis, pH, temperature, molecular weight, pressure, and solvent quality [35, 36]. HPAM is susceptible to mechanical degradation under high shear due to chain scission reducing the polymer chain size and molecular weight, which in turns reduces the viscosity of the polymer solution. Advantages of HPAM are low manufacturing costs and resistance to bacterial attack [36].

Hydrophobically modified polyacrylamides (HMPAMs) are water-soluble polymers containing both hydrophobic groups (e.g., methyl or ethyl acrylates, alkyl vinyl ethers, styrene comonomers, or alkyl acrylamides) and weakly charged pendant groups (e.g., carboxylic acid pendant groups) directly attached to the polymer backbone (**Figure 1(c)**). The hydrophobic groups can be distributed in a block-like fashion, randomly, or discretely distributed along the backbone. In aqueous solutions, these hydrophobic groups aggregate through intra- and intermolecular associations that increase the hydrodynamic volume of the polymer, which increases the viscosity of the polymer solution [36, 38]. The alkyl chain length and charge density determine the hydrophobicity of these polymers [39]. The presence of counter-ions in the aqueous media reduces the repulsion between charged groups within the polymer chain, which favors inter- and intrachain hydrophobic interactions [39, 40]. Benefits of HMPAM include salt tolerance and the enhancement in solution viscosity in the presence of low-molecular-weight electrolytes because of the shielding of intramolecular Coulombic attractions rather than the intermolecular hydrophobic interactions [36]. The inter- and intramolecular hydrophobic interactions are dynamic and reversible. Therefore, under high shear rate, these associations are interrupted and the viscosity of the solution decreases, but as soon as the high mechanical shear is removed, the hydrophobic groups re-associate and the viscosity of the solution returns to its original value [36].

The goal of this exploratory research was to formulate a supramolecular polymer network with enhanced properties (i.e., viscoelasticity, mechanical stability, salt tolerance, and thermal stability), taking advantage of the synergistic combination of the beneficial properties of the individual polymers in the blend. The formation and characterization of the supramolecular polymer network was demonstrated through frequency (time) and temperature-dependent oscillatory rheology [4, 5]; the use of other analytical techniques for structural characterization of the supramolecular system is beyond the scope of this work.

In this chapter, the formulation and characterization of the supramolecular self-assembled polymer network (SAP) is first described, and then the effect of ionic strength on the viscoelastic behavior of the SAP is discussed. The next section describes the structural strength of the SAP through dynamic mechanical analysis (DMA), followed by the evaluation of the SAP thermal stability by dynamic mechanical thermo-analysis (DMTA). In the following section, the long-term thermal stability of the SAP prepared in brines having different ionic strengths is discussed. Finally, the performance of the SAP in displacing heavy oil employing conventional sad-pack displacement tests at simulated oil reservoir conditions is presented.

2. Formulation of the self-assembled polymer network (SAP)

Several types of polymers commercially available were evaluated for the formulation of the SAP network with enhanced viscoelastic flow behavior. Xanthan gum (B), commercial food grade (Groupe Maison Cannelle Inc. (Richmond, QC, Canada)), a partly hydrolyzed polyacrylamide, HPAM, with a degree of hydrolysis ranging from 5 to 10 mol% and a molecular weight of approximately 5×10^6 daltons [41] (GelTech, Midland, TX, USA), and AP of low anionicity, low-molecular weight (8–12 million Dalton), and a high hydrophobic content [42–44] (SNF Floerger, Riceboro, GA, USA). Baseline polymers and polymer blends were initially prepared in brine solution of 2.1 wt% concentration (see **Table 1**). Polymer solutions

were mixed using a magnetic stirrer under strong mixing conditions to prevent the formation of lumps (e.g., fish eyes) at room temperature. The viscoelastic behavior, DMA, and DTMA of the baseline polymers and SAP were characterized through oscillatory rheology at 25°C using a Bohlin Geminin HR Nano Rheometer manufactured by Malvern (Worcestershire, UK) equipped with a parallel-plate measuring geometry (gap: 1000 μm) and a solvent trap to prevent drying effects during measurements. The amplitude sweep was performed in the strain range from 1 to 1000% at a fixed frequency of 1 rad/s, while the frequency sweep was run from 0.01 to 100 rad/s at fixed strain within the linear viscoelastic (LVE) range as determined from the preceding amplitude sweep.

Figure 2 displays the frequency sweeps as the curve functions of the loss factor ($\tan\delta$), storage modulus (G'), loss modulus (G''), and complex viscosity ($|\eta^*|$) for the baseline polymers B, HPAM, and AP at concentrations of 0.2, 0.2, and 0.1 wt%, respectively, prepared in 2.1 wt% brine.

The frequency sweeps (**Figure 2**) demonstrate that all polymers follow the characteristic shear-thinning flow behavior of polymers, thus viscosity decreases with increasing shear rate. At the same salinity (2.1 wt% brine), temperature, and angular frequency range, polymer B at 0.2 wt% solution concentration shows a significantly higher viscoelasticity than the HPAM at 0.2 wt% solution and the AP at 0.1 wt% solution. The behavior of polymer B (i.e., xanthan gum) results from its molecular-ordered aggregation behavior in saline solutions.

Regarding the loss factor ($\tan\delta$), which is useful to describe the viscoelastic behavior of materials in the low shear range ($\omega \leq 1 \text{ s}^{-1}$) [12, 45]; **Figure 2** shows that polymer B behaves different from the HPAM and AP polymer solutions. Polymer B exhibits a flow transition from a viscoelastic liquid behavior ($\tan\delta > 1$) to a viscoelastic weak-gel behavior ($\tan\delta < 1$) as angular frequency increases. At low angular frequencies (i.e., $\omega \leq 1 \text{ rad/s}$), the polysaccharide molecules are entangled with neighboring macromolecules forming aggregates stabilized

Salts	Brine compositions (wt%)		
	2.1	4.2	8.4
NaCl	1.72	3.45	6.9
MgCl ₂	0.04	0.09	0.18
CaCl ₂	0.33	0.65	1.30
Na ₂ SO ₄	0.01	0.02	0.04

Table 1. Brine compositions (wt%).

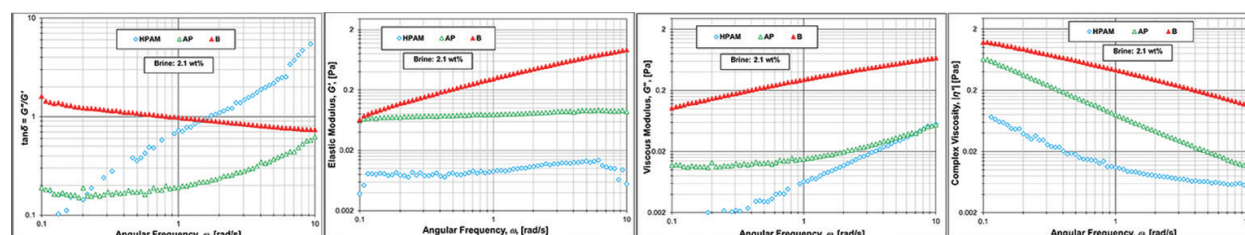
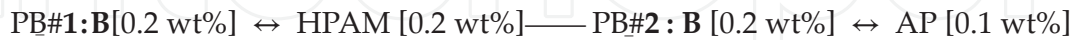


Figure 2. Frequency sweeps as curve functions of $\tan\delta$, G' , G'' , and $|\eta^*|$ for baseline polymers prepared in 2.1 wt% brine.

by hydrogen bonds and intermolecular associations through acetate residues [15] that resist flow and therefore viscous behavior dominates [13, 14, 17, 19, 45]. As the angular frequency increases, progressive disentanglement of the macromolecules takes place aligning the molecules in the direction of shear and shear gradient, which offer less resistance to flow, and the viscoelastic flow behavior of polymer B solution transitions to an elastic-dominated state [11, 12, 17, 20, 45, 46]. This flow behavior at rest and/or low shear is different from the typical flow behavior of common polymer solutions [15–17, 19, 29].

The polymer blends (PBs) and respective concentrations evaluated were as follows:



$\text{PB\#3: HPAM [0.2 wt\%]} \leftrightarrow \text{AP [0.1 wt\%]} \text{---} \text{PB\#4: B [0.2 wt\%]} \leftrightarrow \text{HPAM [0.2 wt\%]} \leftrightarrow \text{AP [0.1 wt\%]}$.

All polymer blend solutions were homogeneous as such phase separation was not observed. The dynamic rheological properties of PB #1, #2, and #4 (**Figure 3**) suggest polymer interactions with an enhanced viscoelasticity relative to the baseline polymers, except for PB #3 (HPAM [0.2 wt%]↔AP [0.1 wt%]) that resulted in far inferior viscoelasticity (data not shown) and was rejected. Besides, it seems that polymer B directs the interactions among the main- and side chains of the blended polymers because PB #1, #2, and #4 assume the rheological behavior of the baseline polymer B (see **Figures 2 and 3**).

Polymer blend #4 -B [0.2 wt%]↔HPAM [0.2 wt%]↔AP [0.1 wt%] showed the highest elasticity and viscosity gain (**Figure 3**). At the angular frequency (ω) of 7.055 rad/s, the percentage increase in $\Delta G'$ was 43%, $\Delta G''$ was 41%, and $\Delta |\eta^*|$ was 42% relative to polymer B baseline. $\Delta G'$, $\Delta G''$, and $\Delta |\eta^*|$ increase by more than an order of magnitude relative to the baseline of the HPAM and AP polymers at the same $\omega = 7.055$ rad/s. Furthermore, the low loss factor, $\tan \delta < 1$, with $G' > G''$ in the entire range of angular frequency; corresponds to a flow behavior that is characteristic of stable dispersions in the form of network-like structures built up through inter- and intramolecular interactions [3, 9, 45, 47–51]. Furthermore, the storage modulus, G' , kept increasing at high angular frequencies, which “[verifies] the dynamic nature of the bonds within the network” [5]. This rheological behavior demonstrates that interchain self-association among the blended polymers forms a stronger polymer network of a larger hydrodynamic volume showing an enhanced solution viscosity. **Figure 3** also shows that PB #1 displays the second larger gain in G' , G'' , and $|\eta^*|$ relative to their individual polymer constituents.

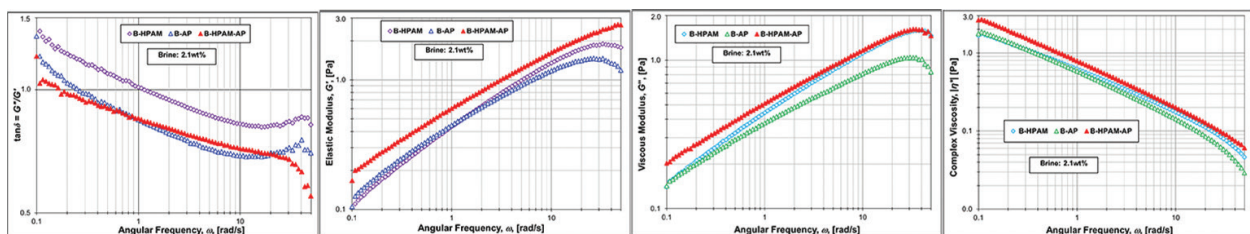


Figure 3. Frequency sweeps as curve functions of $\tan \delta$, G' , G'' , and $|\eta^*|$ for the polymer blends prepared in 2.1 wt% brine.

Supramolecular systems can be formed via electrostatic interactions due to the high solubility of charged groups in water. Previous research has demonstrated that xanthan gum and HPAM form physical networks through ionic cross-linking using divalent cations (e.g., Ca^{2+}) [2, 26]. More examples of network systems built up through electrostatic interactions are reported in Ref. [6]. Specifically, Ca^{2+} is an efficient binder for carboxylic acids that induce aggregation in aqueous polymer solutions through the formation of polyion/cation complexes. In these systems, “the focal point is the carboxylate moiety [that is an] excellent ligand” [52].

In this work, the anionic polymers were mixed in brine containing 3300 ppm of CaCl_2 (see **Table 1**, brine 2.1 wt%). In this system, self-assembling is dominated by rapid cooperative electrostatic interactions in which the divalent cations, Ca^{2+} , bridge the negative charges (i.e., carboxylic groups) in the polymer macromolecules causing complexation of a mixture of anionic polymers. In this case, the divalent cations act as the physical crosslink among the anionic polymer chains [6, 8]. The interpolymer associations driven by electrostatic interactions decrease the intra- and interpolymer electrostatic repulsion promoting the intra- and intermolecular hydrophobic interactions (i.e., van der Waals interactions) among the hydrophobic segments of the macromolecules forming a stronger network structure [36]. Therefore, the screening of the charged groups by divalent cations reduces the steric hindrance among polymer chains and aids the interpolymer association via hydrogen bonding and hydrophobic interactions [53]. Hydrogen bonding among side chains (e.g., carboxylic acids and amide groups) of polymers B, HPAM, and AP takes place, as previously demonstrated between HPAM and xanthan gum side groups [35, 51]. In solution, supramolecular networks are commonly controlled by strong intra- and intermolecular hydrogen bonds. “The double hydrogen bonding of two or more amides can work in a cooperative manner to drive the formation of many ordered supramolecular architectures” [54].

Figure 4 displays the frequency sweep rheometry data that shows the effect of varying the concentration of polymer B in PB # 1 and # 4 from 0.1 to 0.3 wt%, while maintaining the concentrations of HPAM and AP fixed at 0.2 and 0.1 wt%, respectively.

Increasing the concentration of polymer B significantly increases the elasticity and viscosity of both blends. However, the largest gain in viscoelasticity is shown by PB # 4. The rheological data suggest that increasing the concentration of polymer B encourages more intra- and interpolymer chain associations through cation bridging, hydrophobic interactions, and hydrogen bonding, which enhances the structural strength and viscosity of the SAP without compromising its solubility in brine solution [36]. Furthermore, PB # 4 exhibits the lowest

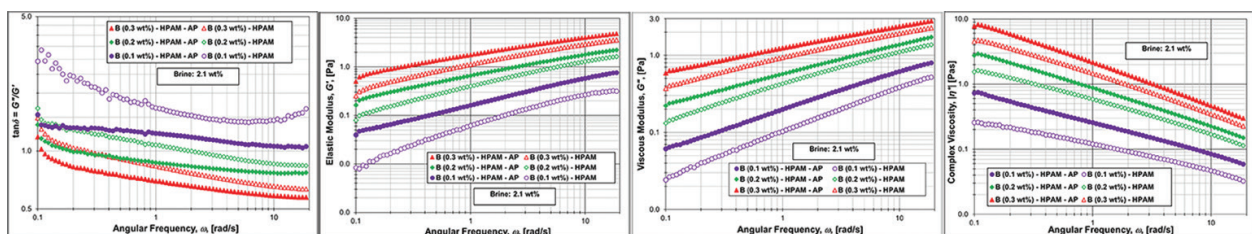


Figure 4. Frequency sweeps as curve functions of $\tan\delta$, G' , G'' , and $|\eta^*|$ for PB # 1 and PB # 4 in 2.1 wt% brine using different concentrations of polymer B in the blends.

crossover point ($G' = G''$ and $\tan\delta < 1$ at $\omega = 0.1$ rad/s), which indicates the formation of a more stable supramolecular system [4]. For this reason, PB # 4 was selected as the optimum SAP formulation. Hereafter, PB # 4 is designated as SAP, while PB # 1 is designated as the baseline system for comparison purposes.

On the basis of the results obtained from oscillatory rheology in this exploratory research, a hypothetical structure of the optimum supramolecular polymer network is proposed in **Figure 5**, which shows the plausible reversible interactions taking place during self-aggregation of the SAP network.

Forthcoming research will characterize the structure of the optimum SAP system in depth, employing several analytical techniques (i.e., ^1H Nuclear Magnetic Resonance ($^1\text{H-NMR}$), Scanning Electron Microscopy (SEM), Fourier Transform Infrared Spectrometry (FTIR), and Size Exclusion Chromatography, among others) to test the proposed hypothetical SAP structure shown in **Figure 5**. In the succeeding section, a qualitative characterization of the polymers and SAP morphologies was conducted through optical microscopy. However, a more comprehensive characterization of these systems is required. This information will be provided in the upcoming work, which is beyond the scope of this chapter.

The morphology of the baseline polymers samples and the optimum SAP was observed using a polarized light optical microscope (Olympus model GX41), equipped with an M Plan N 10 \times /0.25 ∞ -FN22n objective (Olympus), digital camera, and image analysis software (Lumenera model Infinity 2-2C). **Figure 6(a)** and **(b)** display the micrographs of the baseline polymers and SAP dissolved in distilled water and in brine (8.4 wt%), respectively. In these micrographs, **Figures 1–4** correspond to polymers AP, B, HPAM, and SAP respectively.

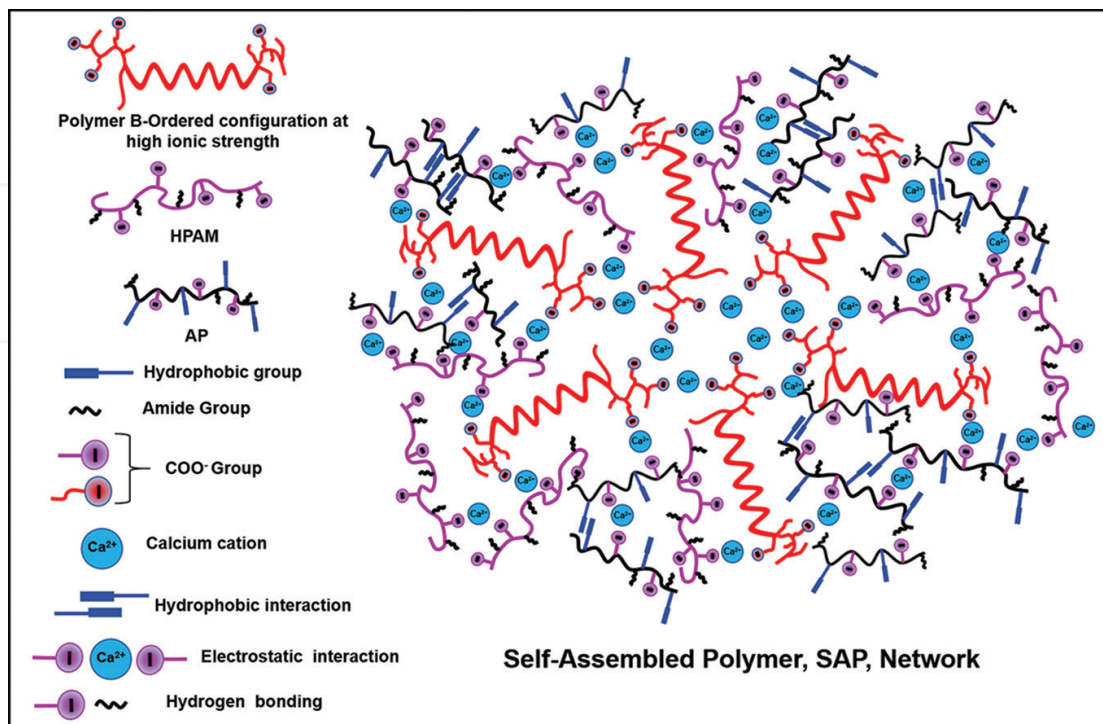


Figure 5. Proposed hypothetical structure of the SAP network.

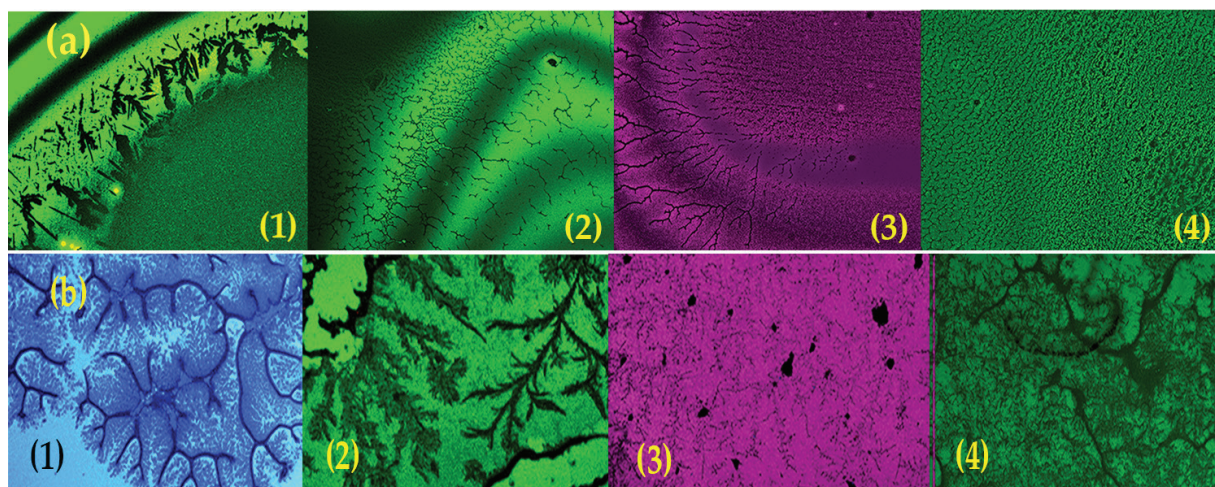


Figure 6. Polarized light micrographs of samples of baseline polymers and SAP system. (a) in distilled water and (b) in brine (8.4 wt%). Micrographs (1)–(4) correspond to polymers AP, B, HPAM, and the SAP system, respectively.

In the photomicrographs presented in **Figure 6(a)** is possible to qualitatively observe the morphology of the different polymer systems despite light interference [55]. The micrograph of the AP polymer in distilled water (**Figure 6(a1)**) reveals well-separated ramifications of aggregated macromolecules or clusters as previously reported for hydrophobically modified polyacrylamides [6, 40], while polymer B (**Figure 6(a2)**), HPAM (**Figure 6(a3)**), and the SAP (**Figure 6(a4)**) display extended macromolecular configurations. The polymer blend in **Figure 6(a4)** exhibits a more dense, well-aligned, and extended configuration of polymer structures. This macromolecular configuration results from the reciprocal charge repulsion among the anionic polymers stretching out the chains, which occupy a larger hydrodynamic volume because, minimum interchain interactions take place in distilled water [13, 26].

Figure 6(b1)–(b4) demonstrate that in brine solution, the screening of the negative charges in the polymer chains causes the increase of intra- and interchain interactions among the anionic polymers. For instance, dense intra- and interchain hydrophobic interactions are visible for the associating polymer, AP, in **Figure 6(b1)**, in the form of a dense network that was not observed in distilled water (**Figure 6(a1)**). Micrographs in **Figure 6(b2)** and **(b3)** display branch-like fractal structures for polymer B and HPAM, which agree with previous research [56]. The screening of the negative charges in the polymer side chains causes the coiling/folding of the polymer chains that decreases the hydrodynamic volume of the macromolecules and the viscosity of the polymer solutions [13, 26]. By contrast, **Figure 6(b4)** exposes a network of fully entangled macromolecules. This high-density thread-like net reveals a homogeneous web of intra- and interchain interactions among the anionic polymers.

3. Effect of ionic strength on the viscoelasticity of the SAP system

Three brine concentrations 2.1, 4.2, and 8.4 wt% (see **Table 1**) were employed to establish the effect of ionic strength on the viscoelasticity of the SAP system. **Figure 7** presents the frequency sweep of the SAP and baseline solutions in different brine concentrations in terms of the curve functions of $\tan\delta$, G' , G'' , and $|\eta^*|$.

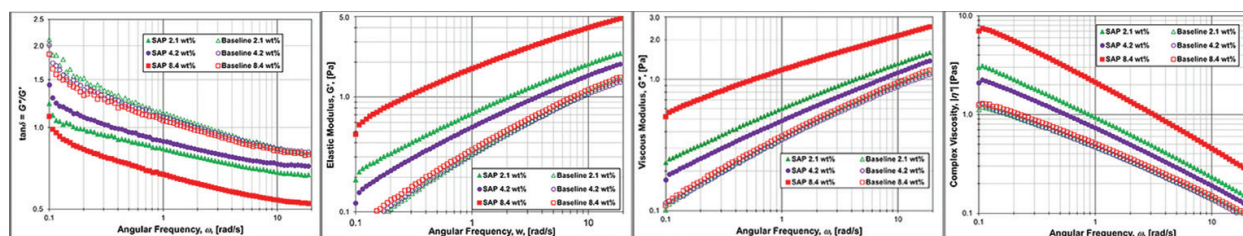


Figure 7. Curves of $\tan\delta$, G' , G'' , and $|\eta^*|$ versus ω and brine concentration.

Figure 7 demonstrates the significant effect of ionic strength on the SAP system. At the highest ionic strength (i.e., brine 8.4 wt%), the SAP system displays the highest elasticity and viscosity. The curves in **Figure 7** show G' values that are markedly larger than G'' at all frequencies. A $\tan\delta < 1$ in the entire range of angular frequency is consistent with a gel (physical network)-like behavior [45]. **Figure 7** also reveals a negligible effect of ionic strength on the viscoelasticity of the baseline or PB # 1, which consists of a mixture of 0.2 wt% polymer **B** and at 0.2 wt% of HPAM.

These rheological data indicate that the higher the ionic strength the higher the suppression of the electrostatic repulsion among polymer chains through cation bridging (i.e., Ca^{2+}), which results in more and stronger intra- and specially interpolymer complexations and associations that reinforce the polymer network and enhances the viscosity of the solution [36]. Previous research has also demonstrated that the addition of inorganic salts to interpolymer mixtures (e.g., anionic and nonionic polymers) in aqueous solutions deteriorates the thermodynamic quality of the solvent (e.g., water) with respect to the polymers, which promotes the strengthening of the interchain complexation through hydrophobic interactions and hydrogen bonding [57].

The main difference between the SAP system and the baseline shown in **Figure 7** is that the SAP system contains 0.1 wt% of AP polymer (i.e., hydrophobically modified polymer); therefore, the addition of inorganic salts shelters the charged groups in the associating polymer side chains and uncovers the hydrophobic moieties, making these associating groups more accessible for intra- and interpolymer hydrophobic interactions [31, 36]. These observations agree with previous work [51].

These experimental findings indicate that the viscoelastic functionality of the SAP formulation is improved as the ionic strength in the aqueous solution increases. This performance makes the SAP system suitable for EOR applications involving brines containing high salinity and hardness concentrations.

4. Dynamic mechanical analysis (DMA)

The structural strength of a material is usually determined through the reestablishment of the storage modulus, G' , of the disrupted network after the shear deformation driven by high shear rates has been lifted [5, 45]. In this study, the structural strength of the SAP system was established through thixotropic behavior analysis by applying an oscillatory rheological test consisting of three steps, each one at constant dynamic mechanical conditions, as recommended in Ref. [45]. The first or *reference* step is carried out at low-shear conditions

(strain = 20%, $\omega = 6.283$ rad/s, time ≈ 960 s) within the LVE range. The G' -value at the end of the first step is taken as the reference value of G' -at-rest to be compared to the G' -value occurring at the end of the third step [45]. The second or *high shear* step is conducted at high shear conditions (strain = 1000%, $\omega = 6.283$ rad/s, time ≈ 480 s) outside the LVE range with the purpose of breaking the internal structure of the sample. The third or *regeneration* step is performed at the same shear conditions (strain = 20%, $\omega = 6.283$ rad/s, time ≈ 960 s) of the first step within the LVE range to facilitate the regeneration of the sample's structure. The percentage of structural regeneration is calculated by taking the G' -value at the end of the third step in relation to the reference value of G' -at-rest of the first step [45].

Figure 8 displays the curves of G' and G'' as a function of time [s], brine concentration (2.1 and 8.4 wt%), and polymer systems for the *reference* step (step 1) and for the *regeneration* step (step 3).

Figure 8 shows that at low salinity (i.e., brine 2.1 wt%), the baseline displays a complete structural regeneration (i.e., thixotropic behavior), while the SAP system exhibits a 5% increase in the structural strength relative to the reference value of G' obtained from step 1. The G' -values (empty square symbols) gathered during the regeneration step are consistently higher than the G' -values (solid square symbols) obtained during the reference step. Furthermore, **Figure 8** indicates that the structural regeneration of both systems takes place immediately after the high shear step ends. The corresponding G'' -curves for both systems show a similar behavior. The mechanical response for both systems is dominated by G' ($\tan\delta < 1$) during the entire testing period, thus displaying a network-like character. The upsurge in the structural strength exhibited by the SAP network is due to the increase in the number and strength of noncovalent interchain associations that reconnect the polymer chains in the network very quickly, causing the rapid regain and enhancement of the mechanical structural strength and solution viscosity [3, 5, 36, 45].

At high brine concentration (i.e., 8.4 wt%), the baseline does not show complete structural regeneration (**Figure 8**). The G' -values obtained in step 3 are below the G' -values obtained in step 1 during the entire testing period. The decrease in the structural strength might be related to the weakening of the interchain noncovalent interactions for this system. On the contrary, the SAP system demonstrates full recovery after extension under load. The G' -values in step 3 show an immediate 100% structural strength regeneration. Again, for the SAP system, $G' > G''$ showing network-like properties during the total testing period.

These results verify the reversibility of the interpolymer interactions of the SAP system involving the instant recovery of the noncovalent associations following shear thinning [58]. This demonstrates the self-healing advantage of supramolecular polymer networks due to the reversibility of the physical associations and high-chain mobility in water [3, 6, 58].

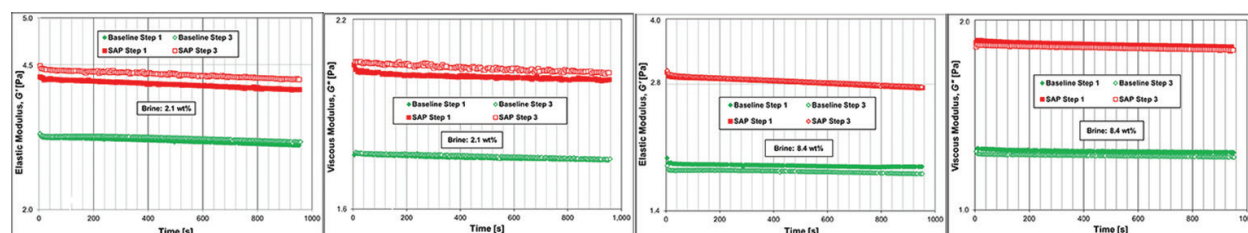


Figure 8. Thixotropic analysis: G' and G'' as a function of time.

5. Dynamic mechanical thermo-analysis (DMTA)

Dynamic mechanical thermo-analysis was conducted by performing upwards temperature ramps from 282.5 (9°C) to 353.5 K (80°C) at a linear heating rate of 9 K/min and downwards temperature ramps from 353.5 (80°C) to 282.5 K (9°C) at a linear cooling rate of 7 K/min at a constant frequency (1 Hz) and % strain (20%) within the LVE range. **Figure 9** displays the oscillatory upward and downward temperature sweeps showing the G' - and G'' -curves of the baseline and SAP network at low- and high salinity.

The upward heating curves (**Figure 9**) show that for both systems (i.e., baseline and SAP network), the G' - and G'' -values decrease as the temperature increases with the G' -values showing steeper curves. Similarly, the downward cooling curves show the reverse process; however, the G' - and G'' -curves show hysteresis upon cooling. As temperature increases during the heating process, the motion and friction between the polymer chains increase, producing frictional heat. A fraction of this frictional heat may heat up the sample and another part may be lost to the surrounding environment; therefore, these materials exhibit irreversible deformation behavior [45] due to heat transfer. **Figure 9** also shows that hysteresis is less pronounced for both systems at higher salinities, which suggests the formation of supramolecular networks that are more rigid, stronger, and more stable at elevated temperatures.

Figure 10 shows that the baseline system reaches the gel transition temperature (T_{gel}) at approximately 334 K (60.5°C) for both brine salinities: 2.1 and 8.4 wt%. As temperature increases, the interchain interactions undergo faster rates of dissociation-association up to the vicinity of the gel transition temperature at which the rate of dissociation is much higher than the rate of association. At T_{gel} , disruption of the network takes place and the system transitions from a gel-like flow behavior to a fluid-like flow behavior [9, 58]. Likewise, during the cooling process as temperature decreases, the rate of interchain dissociation-association decreases and chain interactions get progressively stronger and the material becomes more elastic until $G' = G''$ at the crossover point, the flow gel-like behavior is regained and $G' > G''$ at lower temperatures [45].

The SAP system displays a different behavior as shown in **Figure 10**. In both brine salinities (2.1 and 8.4 wt%), the heating curves do not reach the gel transition temperatures. At low salinity, the cooling curve just reaches the crossover point ($G' = G''$ and $\tan\delta = 1$) at the highest testing temperature and then rapidly transitions to a viscoelastic gel behavior upon cooling. The SAP cooling curve at a high salinity never reaches the transition temperature ($G' = G''$). These observations suggest that the SAP network exhibits more rigid and stronger polymer

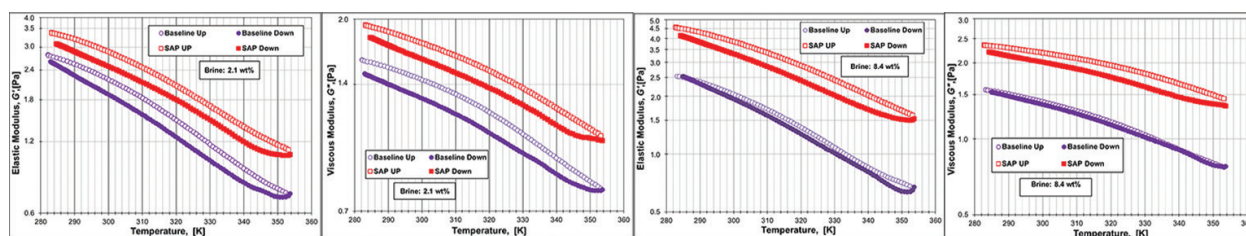


Figure 9. Temperature-dependent functions of G' and G'' of baseline and SAP network.

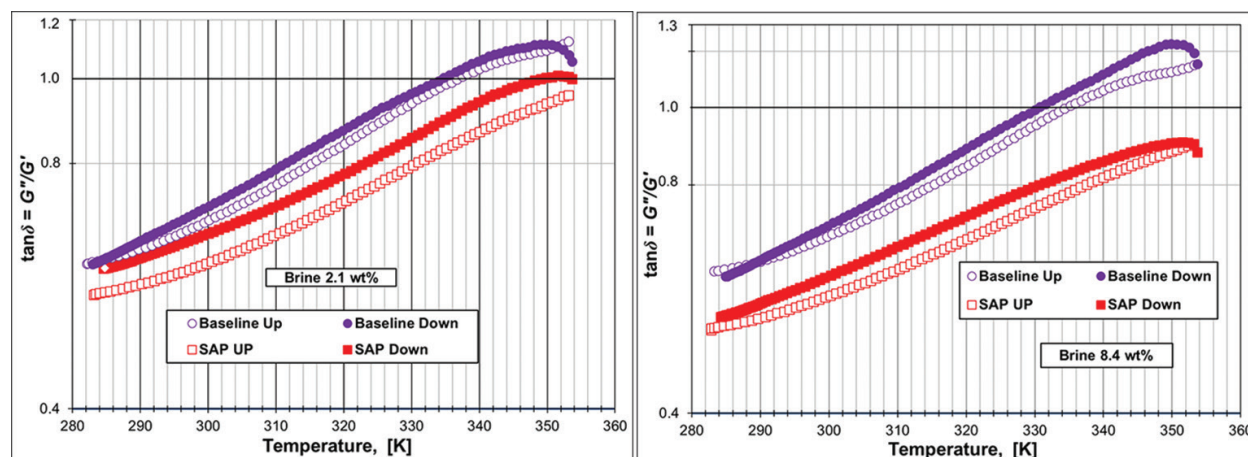


Figure 10. Temperature-dependent function of $\tan\delta$ of the baseline and SAP system.

chain interactions, which are capable of maintaining the stability of the supramolecular polymer network and the behavior of a viscoelastic gel ($G' > G''$) in the range of temperature evaluated. Therefore, the interchain associations are stable and network disruption was not observed in the temperature range from 282.5 (9°C) to 353.5 K (80°C) [45, 58].

6. Extended thermal stability

The extended thermal stability evaluation was performed at 90°C for a period of 8 weeks. **Figure 11** displays the G' - and G'' -curves versus angular frequency and time of the baseline and SAP system at low- and high-salinity brines.

The G' - and G'' -curves (**Figure 11**) indicate that after the second week (Week # 2) of testing, the elasticity and viscosity of the baseline and the SAP network are significantly affected. At low-salinity brine (2.1 wt%), the baseline displays a more stable performance than the SAP network during the testing period; however, this behavior is reversed at high-salinity brine concentration (8.4 wt%), in which the SAP system is noticeably more stable, particularly at week # 8, than the baseline system. Furthermore, the direct observation of the samples reveals the onset of fine solid precipitation from week # 2 for both systems and brine concentrations. Some of the samples became turbid with testing time.

The thermal deterioration of the viscoelasticity of both systems as a function of time could be attributed in part to the autohydrolysis of the amide moieties (i.e., acrylamide groups) and hydrophobic functional groups forming additional acrylate moieties at elevated temperatures (i.e., >85°C). These acrylate structures rapidly associate with divalent cations (i.e., Ca^{2+}) causing the precipitation of polymer from the bulk of the solution, which becomes turbid. More detailed information on autohydrolysis of polymers at elevated temperature and ionic strength is provided elsewhere [43, 59]. Thermal degradation of the polymer samples can also be attributed to the induced breaking of the acrylic backbone trigger via free-radical reactions, which reduces the molecular weight of the polymer chains [59].

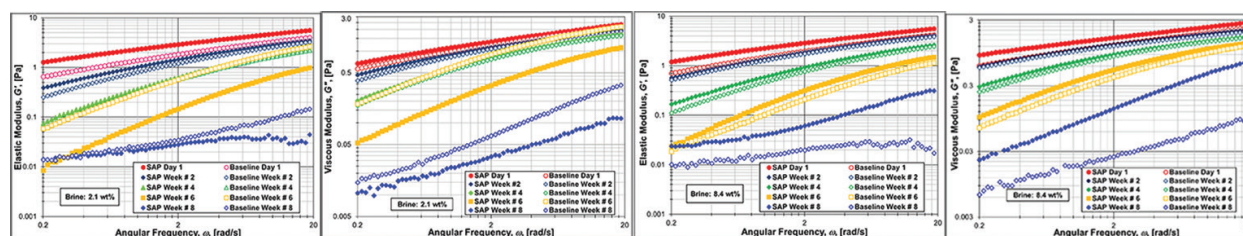


Figure 11. G' - and G'' -curves as a function of angular frequency and time.

Although this extended thermal stability evaluation demonstrates the significant effect of temperature and time on the viscoelastic **flow** behavior of both systems, these results further confirm that the functionality of the SAP system is increased at higher ionic strengths due to the formation of stronger intra- and interpolymer associations that enhances its stability at 90°C.

7. Heavy oil recovery

The performance of the baseline and the SAP system as mobility control agents in displacing and mobilizing heavy oil was carried out through conventional sand-pack displacement tests. The heavy oil that was provided by Husky Energy Inc. (Calgary, AB, Canada) had an initial viscosity of 68,728 cP at 25°C that was adjusted to 3000 cP at 25°C by dilution with natural condensate (density: 0.9 g/ml) provided by Corridor Resources Inc. (McCully field, Sussex, NB, Canada). A Temco DCHH-series core holder (Temco Inc., Tulsa, OK, USA) was employed to perform the displacement tests. The core holder's rubber sleeve was packed with sand (QUIKRETE® Premium Play Sand®, No. 1113, 100% quartz) of effective size: $D_{10} = 180 \mu\text{m}$ and a uniformity coefficient: $D_{60}/D_{10} = 2.44$ determined by sieve analysis (ASTM C136/C136M-14) [60] employing woven wire brass sieves (Endecotts Limited, London, UK). The packed sleeve was sealed using the floating distribution plug and inserted into the core holder body. An overburden pressure of 500 psi was applied by filling the annulus between the outer diameter of the sleeve and the inner diameter of the core holder body with distilled water. CFR-series transfer vessels (Temco Inc., Tulsa, OK, USA) were used to store heavy oil, brine, and polymer that were pumped to the sand pack by a Teledyne ISCO Syringe pump, model 100DX (Teledyne Isco Inc., Lincoln, NE, USA). Pressure gauges (Omega, Laval, QC, Canada) with an accuracy of 0.5% (FS) were installed in different sections of the sand-pack displacement setup (Figure 12).

Four displacement tests were carried out at 25°C. Two displacement tests evaluated the performance of the baseline system and the other two tests the performance of the SAP network. The unconsolidated porous media were characterized by determining the pore volume (PV), porosity (ϕ), and permeability (k) following standard procedures described in Ref. [61]; at this stage, the sand packs were 100% saturated with brine (8.4 wt%). Table 2 summarizes the properties of each of the sand packs employed during the flooding tests.

The fluid injection sequence was carried out in four steps as follows. The first step was the injection of heavy oil into the brine-saturated porous media until no more brine was produced from the sand pack that corresponded to approximately two pore volumes (2PV), followed by

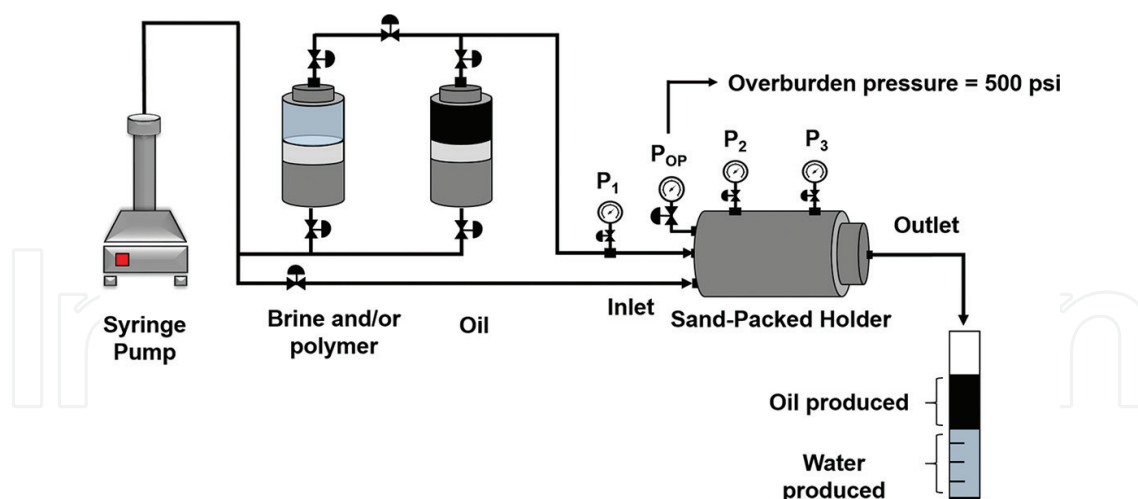


Figure 12. Experimental setup sand-pack displacement test.

Flooding test #	Pore volume, PV (cm ³)	Porosity, ϕ (%)	Permeability, k (mD)
Baseline # 1	208	29	10,049
Baseline # 2	206	29	8667
SAP # 1	204	29	8109
SAP # 2	187	26	4700

Table 2. Sand-pack properties.

the second step of brine (8.4 wt%) injection to displace heavy oil (i.e., water flooding) until the production of oil stopped, which corresponded on average to the injection of 6 PVs of brine. The third step consisted of the injection of 1 PV of baseline and/or the SAP system as EOR mobility control agents to further displace and recover oil. The fourth and final step was the post-polymer brine (8.4 wt%) injection as a chaser to displace the baseline polymer and/or the SAP system through the sand pack. On average, 6PV of post-polymer brine was injected. The average injection flow rate was 0.76 ml/min that corresponds to a linear velocity of 0.77 ft./day. During each injection step, the volume of fluid injected, the volume of fluid produced, injection time, and pressures at the inlet, at the sand-pack pressure ports, and outlet of the sand-pack holder were recorded. Material balance of each injection step was carried out to determine the sand-pack fluid saturation and oil recovery. More details on the experimental procedure employed during these routine sand-pack displacement tests are provided in Ref. [62].

The performance of the baseline and the SAP network as mobility control agents in porous media was analyzed by plotting the effective viscosity or resistance factor (RF) [63–68] of the polymer system during flow through porous media as a function of the volume of fluid injected expressed as a fraction of pore volume (PV), which was normalized for porosity and permeability to compare the displacement tests on the same reference. The capillary bundle parameter model was applied for data normalization [66, 69–71].

Polymer retention in porous media after the post-polymer brine injection was determined by the residual resistance factor, RRF [59, 62–65, 67, 68, 70–74]. RF and RRF are significant parameters because they provide reliable information on the propagation and effectiveness of polymeric systems as mobility control agents through porous media. **Figure 13** displays the average RF and RRF as a function of the volume of fluid injected normalized for porosity and permeability of the baseline and the SAP system sand-pack displacement tests.

The RF curves reveal that the SAP system offers a higher end value of effective viscosity, RF (61%), during flow in porous media relative to the baseline. The SAP RF curve also shows a tendency to level off as a function of the volume of fluid injected, which indicates an appropriate propagation of the SAP network through the unconsolidated porous media. Therefore, the SAP network displays a better performance as mobility control agent compared with the baseline system.

The RRF curves indicate a larger retention of the SAP system along the sand pack with an end RRF value that stabilizes at around 2.8, while the end RRF value induced by the baseline levels off at approximately 1.3. Therefore, the permeability of the unconsolidated sand packs was further reduced by the SAP system, which aids the displacement and mobilization of heavy oil by further reducing the relative permeability to water [70, 75].

Figure 14 shows cumulative oil recovery as the percentage of the original oil in place (OOIP) recovered, the ratio of the remaining oil saturation to the initial oil saturation (S_{or}/S_{oi}), and the water to oil ratio (WOR) as a function of the volume of fluid injected for the water-flooding stage, polymer-flooding stage, and post-polymer water-flooding stage. Water flooding as a secondary oil recovery process on average recovers between 20 and 30% of the original oil in place [76, 77], which agree with our results.

Polymer-flooding and the post-polymer water-flooding steps rendered an overall percentage of cumulative oil recovery of 41% for the baseline system and 51% for the SAP network. Therefore, the SAP system rendered a 10% higher incremental oil recovery relative to the baseline. In field applications of polymer flooding, an incremental oil recovery of 5% is considered successful [44].

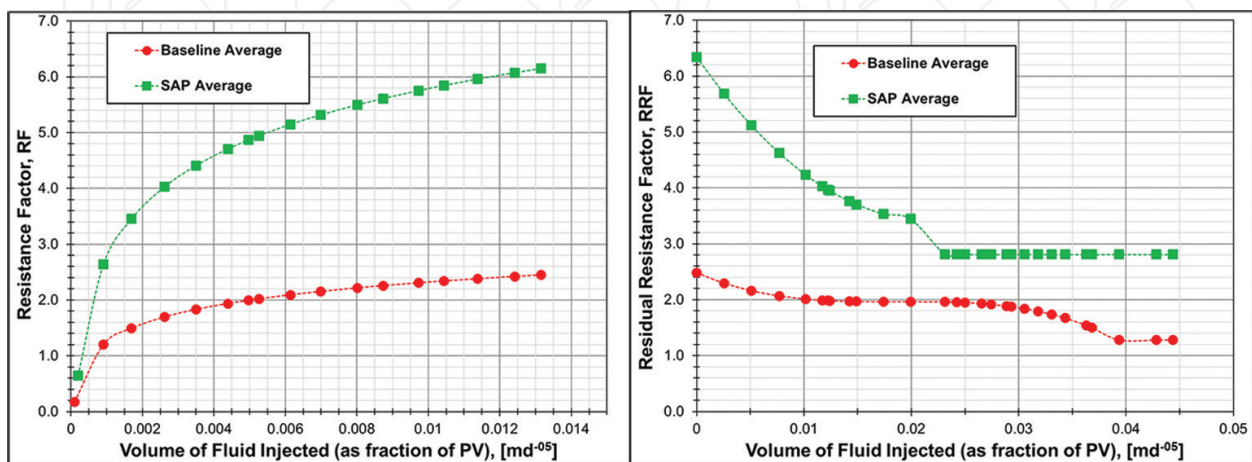


Figure 13. RF and RRF versus volume of fluid injected.

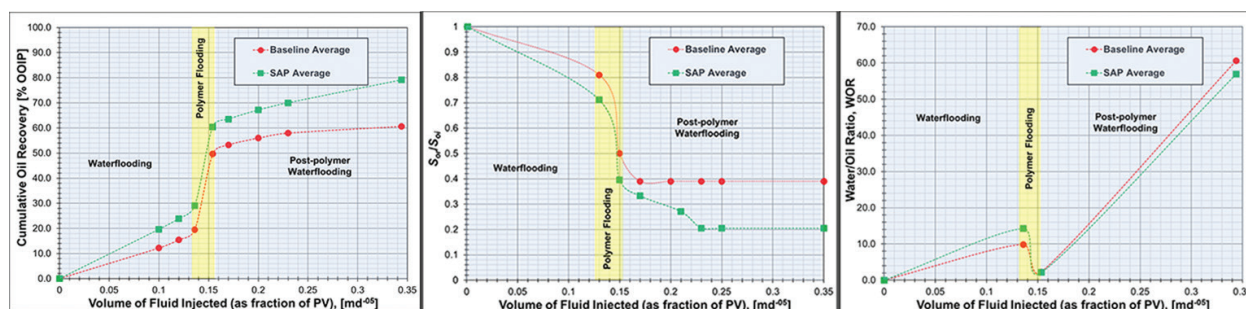


Figure 14. Cumulative oil recovery, S_{or}/S_{or}^i and WOR versus volume of fluid injected.

The superior performance of the SAP network in displacing heavy oil is attributed to an enhanced effective viscosity during flow in porous media, which generates a more stable displacement front that increases the volumetric sweep efficiency accelerating the production of oil. Besides, both systems—the baseline and the SAP network—show to be very efficient in controlling WOR during the polymer-flooding stage. However, as soon as the post-polymer water flooding is initiated, the water to oil ratio, WOR, increases very rapidly, due to the uncontrollable channeling of brine toward the production end caused by viscous fingering [63].

8. Conclusions

A stable supramolecular system was formulated based on the self-assembling of xanthan gum, HPAM, and HMPAM driven by electrostatic interactions through divalent cation (i.e., Ca^{2+}) bridges, which reduce the steric hindrance among anionic polymer chains promoting strong and stable intra- and interpolymer associations via hydrophobic interactions and hydrogen bonding. The viscoelastic functionality of the SAP system is enhanced in high ionic strength aqueous solutions. This performance makes the SAP system suitable for EOR applications involving brines containing high salinity and hardness concentrations.

The SAP system shows a high structural strength, mechanical stability, and self-healing capabilities. The supramolecular polymer network exhibits instant recovery of the interpolymer noncovalent interactions and even the increase in structural strength following the lifting of high-shear conditions (i.e., severe shear thinning).

In the temperature range from 282.5 (9°C) to 353.5 K (80°C), the SAP network exhibits thermal stability. In this temperature range, the strong and stable intra- and interchain interactions maintain the integrity of the supramolecular polymer and its flow viscoelastic behavior. Likewise, the SAP system demonstrated an enhanced thermal stability after 8 weeks at 90°C in high-salinity brine (8.4 wt%) compared with the thermal performance of the baseline. This further confirms that the functionality of the SAP system is upgraded at higher ionic strengths due to the formation of stronger intra- and interpolymer associations.

The SAP system rendered a 10% higher incremental oil recovery relative to the baseline system. The superior performance of the SAP network in displacing heavy oil is attributed to better mobility control properties, to the generation of a stable displacement front, the

efficient and rapid control of the WOR, and an improved volumetric sweep efficiency that accelerates the production of oil. Overall, the SAP system is a straightforward formulation that offers several advantages relevant to EOR such as enhanced viscoelastic flow behavior, increased functionality in high ionic strength environments, stability to mechanical shear, and an improved thermal stability.

Acknowledgements

The authors would like to extend their appreciation to Dr. Chutima Kongvarhodom, Department of Chemical Engineering, Faculty of Engineering, King Mongkut's University of Technology Thonburi (KMUTT), Thoongkru, Bangkok, Thailand, for leading the academic exchange program between KMUTT and the University of New Brunswick (UNB). Likewise, the authors gratefully acknowledge GelTech, SNF Floerger, Husky Energy, and Corridor Resources Inc. for providing samples of polymers, heavy oil, and condensate. The authors would like to acknowledge financial support from the UNB through the Sabbatical Research Grant and the Canada Foundation for Innovation, CFI, research grant.

Author details

Laura Romero-Zerón^{1*} and Saran Banthong²

*Address all correspondence to: laurarz@unb.ca

1 Chemical Engineering Department, Faculty of Engineering, University of New Brunswick, Fredericton, New Brunswick, Canada

2 Chemical Engineering Department, Faculty of Engineering, King Mongkut's University of Technology Thonburi, Bangkok, Thailand

References

- [1] Zhang C. Flow enabled self assembly of polymers [Doctoral dissertation]. Georgia Institute of Technology: Atlanta; 2016
- [2] Lowe AB, McCormick CL. Stimuli responsive water-soluble and amphiphilic (co)polymers. In: McCormick CL, editor. Stimuli-Responsive Water Soluble and Amphiphilic Polymers. Washington: American Chemical Society; 2001. pp. 1-13. DOI: 10.1021/bk-2001-0780
- [3] Aida T, Meijer EW, Stupp SI. Functional supramolecular polymers. *Science*. 2012; **335**:813-817
- [4] Chen S, Döhler D, Binder WH. Rheology of hydrogen-bonded dendritic supramolecular polymer networks in the melt state. *Polymer*. 2016;**107**:466-473

- [5] Yan T, Schröter K, Herbst F, Binder WH, Thurn-Albrecht T. Unveiling the molecular mechanism of self-healing in a telechelic, supramolecular polymer network. *Scientific Reports*. 2016;**6**:32356
- [6] Voorhaar L, Hoogenboom R. Supramolecular polymer networks: Hydrogels and bulk materials. *Chemical Society Reviews*. 2016;**45**(14):4013-4031
- [7] Mendes AC, Baran ET, Reis RL, Azevedo HS. Fabrication of phospholipid-xanthan microcapsules by combining microfluidics with self-assembly. *Acta Biomaterialia*. 2013;**9**(5):6675-6685
- [8] Shchipunov Y, Sarin S, Kim I, Ha CS. Hydrogels formed through regulated self-organization of gradually charging chitosan in solution of xanthan. *Green Chemistry*. 2010;**12**(7):1187-1195
- [9] Brunsveld L, Folmer BJ, Meijer EW, Sijbesma RP. Supramolecular polymers. *Chemical Reviews*. 2001;**101**(12):4071-4098
- [10] Gyarmati B, Pukánszky B. Natural polymers and bio-inspired macromolecular materials. *European Polymer Journal*. 2017;**93**:612-617
- [11] Xu L, Xu G, Liu T, Chen Y, Gong H. The comparison of rheological properties of aqueous welan gum and xanthan gum solutions. *Carbohydrate Polymers*. 2013;**92**(01):516-522
- [12] Cunha RL, Maialle KG, Menegalli FC. Evaluation of the drying process in spouted bed and spout fluidized bed of xanthan gum: Focus on product quality. *Powder Technology*. 2000;**7**(03):234-242
- [13] Baumgartner S, Pavli M, Kristl J. Effect of calcium ions on the gelling and drug release characteristics of xanthan matrix tablets. *European Journal of Pharmaceutics and Biopharmaceutics*. 2008;**69**(02):698-707
- [14] Sereno NM, Hill SE, Mitchell JR. Impact of the extrusion process on xanthan gum behaviour. *Carbohydrate Research*. 2007;**342**(10):1333-1342
- [15] Song KW, Kim YS, Chang GS. Rheology of concentrated xanthan gum solutions: Steady shear flow behavior. *Fibers and Polymers*. 2006;**7**(02):129-138
- [16] Garcia-Ochoa F, Santos VE, Casas JA, Gomez E. Xanthan gum: Production, recovery, and properties. *Biotechnology Advances*. 2000;**18**(7):549-579
- [17] Katzbauer B. Properties and applications of xanthan gum. *Polymer Degradation and Stability*. 1998;**59**(1-3):81-84
- [18] Casas JA, Santos VE, Garcia-Ochoa F. Xanthan gum production under several operational conditions: Molecular structure and rheological properties. *Enzyme and Microbial Technology*. 2000;**26**(2-4):282-291
- [19] Cuvelier G, Launay B. Concentration regimes in xanthan gum solutions deduced from flow and viscoelastic properties. *Carbohydrate Polymers*. 1986;**6**(5):321-333
- [20] Rodd AB, Dunstan DE, Boger DV. Characterisation of xanthan gum solutions using dynamic light scattering and rheology. *Carbohydrate Polymers*. 2000;**42**(02):159-174

- [21] Holzwarth G. Molecular weight of xanthan polysaccharide. *Carbohydrate Research*. 1978; **66**(01):173-186
- [22] Boyd MJ, Hampson FC, Jolliffe IG, Dettmar PW, Mitchell JR, Melia CD. Strand-like phase separation in mixtures of xanthan gum with anionic polyelectrolytes. *Food Hydrocolloids*. 2009;**23**(08):2458-2467
- [23] Viebke C. Order-disorder conformational transition of xanthan gum. In: Dumitriu S, editor. *Polysaccharides: Structural Diversity and Functional Versatility*. 2nd ed. New York: CRC press; 2004. 1189 p
- [24] Mendes AC, Strohmenger T, Goycoolea F, Chronakis IS. Electrostatic self-assembly of polysaccharides into nanofibers. *Colloids and Surfaces, A: Physicochemical and Engineering Aspects*. 2017;**531**:182-188
- [25] Merino-González A, Kozina A. Influence of aggregation on characterization of dilute xanthan solutions. *International Journal of Biological Macromolecules*. 2017;**105**:834-842
- [26] Kumar A, Rao KM, Han SS. Application of xanthan gum as polysaccharide in tissue engineering: A review. *Carbohydrate Polymers*. 2018;**180**:128-144
- [27] Pastuszka MK, MacKay JA. Engineering structure and function using thermoresponsive biopolymers. *Nanomedicine and Nanobiotechnology*. 2016;**8**(01):123-138
- [28] Kim J, Hwang J, Kang H, Choi J. Chlorhexidine-loaded xanthan gum-based biopolymers for targeted, sustained release of antiseptic agent. *Journal of Industrial and Engineering Chemistry*. 2015;**32**:44-48
- [29] Milas M, Rinaudo M, Knipper M, Schuppiser JL. Flow and viscoelastic properties of xanthan gum solutions. *Macromolecules*. 1990;**23**(09):2506-2511
- [30] Camesano TA, Wilkinson KJ. Single molecule study of xanthan conformation using atomic force microscopy. *Biomacromolecules*. 2001;**2**(04):1184-1191
- [31] Hidalgo ME, Armendariz M, Wagner JR, Risso PH. Effect of xanthan gum on the rheological behavior and microstructure of sodium caseinate acid gels. *Gels*. 2016;**2**(03):23
- [32] Williams PA, Day DH, Langdon MJ, Phillips GO, Nishinari K. Synergistic interaction of xanthan gum with glucomannans and galactomannans. *Food Hydrocolloids*. 1991;**4**(06):489-493
- [33] Cairns P, Miles MJ, Morris V. Intermolecular binding of xanthan gum and carob gum. *Nature*. 1986;**322**:89
- [34] Becker A, Katzen F, Pühler A, Ielpi L. Xanthan gum biosynthesis and application: A biochemical/genetic perspective. *Applied Microbiology and Biotechnology*. 1998;**50**(02):145-152
- [35] Cai S, He X, Liu K, Rodrigues AM, Zhang R. Macromolecular interactions and synergy in xanthan/HPAM aqueous solutions. *RSC Advances*. 2017;**7**(66):41630-41639

- [36] Wever DA, Picchioni F, Broekhuis AA. Polymers for enhanced oil recovery: A paradigm for structure–property relationship in aqueous solution. *Progress in Polymer Science*. 2011;**36**(11):1558-1628
- [37] Xin X, Xu G, Gong H, Bai Y, Tan Y. Interaction between sodium oleate and partially hydrolyzed polyacrylamide: A rheological study. *Colloids and Surfaces, A: Physicochemical and Engineering Aspects*. 2008;**326**(1-2):1-9
- [38] Semenov AN, Rubinstein M. Dynamics of entangled associating polymers with large aggregates. *Macromolecules*. 2002;**35**(12):4821-4837
- [39] Tonge SR, Tighe BJ. Responsive hydrophobically associating polymers: A review of structure and properties. *Advanced Drug Delivery Reviews*. 2001;**53**(01):109-122
- [40] Yang ZL, Gao BY, Li CX, Yue QY, Liu B. Synthesis and characterization of hydrophobically associating cationic polyacrylamide. *Chemical Engineering Journal*. 2010;**161**(1-2):27-33
- [41] Seright RS. Gel propagation through fractures. *SPE Production & Facilities*. 2001;**16**(04):225-231
- [42] SNF Floerger. Enhancing Polymer Flooding Performance. 30 years of Experience in EOR [Internet]. 2018. Available from: http://www.snfoil.com/images/phocagallery/brochures/SNF_in_chemical_enhanced_oil_recovery.pdf. [Accessed: 2018-01-29]
- [43] Levitt D, Pope GA. Selection and screening of polymers for enhanced-oil recovery. In: *SPE Symposium on Improved Oil Recovery*; 19-23 April 2008; Tulsa, Oklahoma: SPE; 2008. pp. 1-18
- [44] Perttamo EK. Characterization of Associating Polymer (AP) Solutions. Influences on flow behavior by the degree of hydrophobicity and salinity [thesis]. The University of Bergen; 2013
- [45] Mezger TG. *The Rheology Handbook*. 4th ed. Vincentz Network: Hanover; 2014
- [46] Talukdar MM, Vinckier I, Moldenaers P, Kinget R. Rheological characterization of xanthan gum and hydroxypropylmethyl cellulose with respect to controlled-release drug delivery. *Journal of Pharmaceutical Sciences*. 1996;**85**(05):537-540
- [47] Clausen TM, Vinson PK, Minter JR, Davis HT, Talmon Y, Miller WG. Viscoelastic micellar solutions: Microscopy and rheology. *Physical Chemistry*. 1992;**96**(01):474-484
- [48] Kitazawa Y, Ueki T, McIntosh LD, Tamura S, Niitsuma K, Imaizumi S, Lodge TP, Watanabe M. Hierarchical sol-gel transition induced by thermosensitive self-assembly of an ABC triblock polymer in an ionic liquid. *Macromolecules*. 2016;**49**(04):1414-1423
- [49] Herrera MP, Vasanthan T. Rheological characterization of gum and starch nanoparticle blends. *Food Chemistry*. 2018;**243**:43-49
- [50] Wang Y, Zhong M, Park JV, Zhukhovitskiy AV, Shi W, Johnson JA. Block co-polyMOCs by stepwise self-assembly. *Journal of the American Chemical Society*. 2016;**138**(33):10708-10715

- [51] Lewis CL, Stewart K, Anthamatten M. The influence of hydrogen bonding side-groups on viscoelastic behavior of linear and network polymers. *Macromolecules*. 2014; **47**(02):729-740
- [52] Steed JW, Atwood JL. *Supramolecular Chemistry*. John Wiley & Sons; 2013
- [53] Chen S, Binder WH. Dynamic ordering and phase segregation in hydrogen-bonded polymers. *Accounts of Chemical Research*. 2016; **49**(7, 07):1409-1420
- [54] Zhang D-W, Wang H, Li Z-T. Hydrogen bonding motifs: New progresses. In: Wu L-Z, Li Z-T, editors. *Hydrogen Bonded Supramolecular Structures*. New York: Springer Heidelberg; 2015. p. 350
- [55] Carlton RA. *Polarized Light Microscopy. Pharmaceutical Microscopy*. New York: Springer; 2011. pp. 7-64
- [56] Chen YL, Yuan JH, Yang WH, Huang DH, Tan H, Fei Q. Self-assembly fractal microstructures of HPAM/chromium acetate and HPAM/phenolic aldehyde colloidal dispersion gel. *Journal of Dispersion Science and Technology*. 2003; **24**(01):113-121
- [57] Khutoryanskiy VV, Mun GA, Nurkeeva ZS, Dubolazov AV. pH and salt effects on interpolymer complexation via hydrogen bonding in aqueous solutions. *Polymer International*. 2004; **53**(09):1382-1387
- [58] Yu X, Chen X, Chai Q, Ayres N. Synthesis of polymer organogelators using hydrogen bonding as physical cross-links. *Colloid & Polymer Science*. 2016; **294**(01):59-68
- [59] Levitt D-B. *The optimal use of enhanced oil recovery polymers under hostile conditions [Doctoral dissertation]*. Austin: The University of Texas; 2009
- [60] University, The Ohio State. *Sand Size Analysis for Omsite Wastewater Treatment Systems. Determination of Sand Effective Size and Uniformity Coefficient [Internet]*. Available from: <https://ohioline.osu.edu/factsheet/aex-757>. [Accessed: August 18, 2017]
- [61] McPhee C, Reed J, Zubizarreta I. *Core Analysis: A Best Practice Guide*. Waltham: Elsevier; 2015
- [62] Riahinezhad M, Romero-Zerón L, McManus N, Penlidis A. Evaluating the performance of tailor-made water-soluble copolymers for enhanced oil recovery polymer flooding applications. *Fuel*. 2017; **203**:269-278
- [63] Seright RS. How much polymer should be injected during a polymer flood? Review of previous and current practices. *SPE Journal*. 2017; **22**(01):1-8
- [64] Dupuis G, Rousseau D, Tabary R, Grassl B. Flow of Hydrophobically modified water-soluble polymers in porous media: Controlled resistance factors vs. flow-induced gelation in the Semidilute regime. *SPE Journal*. 2012; **17**(04):1196-1206
- [65] Pancharoen M, Thiele MR, Kovscek AR. Inaccessible pore volume of associative polymer floods. In: *SPE Improved Oil Recovery Symposium*; 24-28 April, 2010. Tulsa, Oklahoma: SPE; 2010. pp. 1-15

- [66] Seright RS, Fan T, Wavrik K, Wan H, Gaillard N, Favéro C. Rheology of a new sulfonic associative polymer in porous media. *SPE Reservoir Evaluation & Engineering*. 2011;**14**(06):726-734
- [67] Kazempour M, Sundstrom EA, Alvarado V. Effect of alkalinity on oil recovery during polymer floods in sandstone. *SPE Reservoir Evaluation & Engineering*. 2012;**15**(02):195-209
- [68] Manichand RN, Seright R. Field vs. laboratory polymer-retention values for a polymer flood in the tambaredjo field. *SPE Reservoir Evaluation & Engineering*. 2014;**17**(03):314-325
- [69] Civan F. *Porous Media Transport Phenomena*. John Wiley & Sons; 2011
- [70] Seright RS. *Use of Polymers to Recover Viscous Oil from Unconventional Reservoirs*. US Department of Energy. Final Report. Contract No. DE-NT0006555; 2011
- [71] Taylor KC, Nasr-El-Din HA. Water-soluble hydrophobically associating polymers for improved oil recovery: A literature review. *Journal of Petroleum Science and Engineering*. 1998;**19**(03):265-280
- [72] Li K, Sun W, Li F, Qu Y, Yang Y. Novel method for characterizing single-phase polymer flooding. *SPE Journal*. 2014;**19**(04):695-702
- [73] Lotfollahi M, Farajzadeh R, Delshad M, Al-Abri AK, Wassing BM, Al-Mjeni R, Awan K, Bedrikovetsky P. Mechanistic simulation of polymer injectivity in field tests. *SPE Journal*. 2016;**21**(04):1178-1191
- [74] Quadri SM, Shoaib M, AM AS, Alhassan SM. Screening of polymers for EOR in high temperature, high salinity and carbonate reservoir conditions. In: *International Petroleum Technology Conference*; 6-9 December, 2015; Doha, Qatar. Vol. 2015. pp. 1-30
- [75] Sheng JJ, Leonhardt B, Azri N. Status of polymer-flooding technology. *Journal of Canadian Petroleum Technology*. 2015;**54**(02):116-126
- [76] Satter A, Iqbal GM, Buchwalter JL. *Practical Enhanced Reservoir Engineering: Assisted with Simulation Software*. Tulsa: Pennwell Books; 2007
- [77] Levitt D, Pope GA. Selection and screening of polymers for enhanced-oil recovery. In: *SPE Symposium on Improved Oil Recovery*; 19-23 April 2008. Tulsa, Oklahoma: SPE; 2008. pp. 1-18

